Title

Spatial and Temporal Correlations of XY Macro Spins

Journal

Nano Letters, 18(12)

ISSN

1530-6984

Authors

Streubel, Robert
Kent, Noah
Dhuey, Scott
et al.

Publication Date

2018-12-12

DOI

10.1021/acs.nanolett.8b01789

Peer reviewed

Spatial and Temporal Correlations of XY Macro Spins

Robert Streubel,[*,†] Noah Kent,[†,‡] Scott Dhuey,[¶] Andreas Scholl,[§] Steve Kevan,[§,‖] and Peter Fischer[†,‡]

†*Materials Sciences Division, Lawrence Berkeley National Laboratory, Berkeley CA 94720, USA*

‡*Physics Department, UC Santa Cruz, Santa Cruz CA 95064, USA*

¶*Molecular Foundry, Lawrence Berkeley National Laboratory, Berkeley CA 94720, USA*

§*Advanced Light Source, Lawrence Berkeley National Laboratory, Berkeley CA 94720, USA*

‖*Department of Physics, University of Oregon, Eugene, OR 97401, USA*

E-mail: streubel@lbl.gov

Abstract

We use nano disk arrays with square and honeycomb symmetry to investigate magnetic phases and spin correlations of XY dipolar systems at the micro scale. Utilizing magnetization sensitive x-ray photoemission electron microscopy, we probe magnetic ground states and the "order-by-disorder" phenomenon predicted 30 years ago. We observe the antiferromagnetic striped ground state in square lattices, and six-fold symmetric structures, including trigonal vortex lattices and disordered floating vortices, in the honeycomb lattice. The spin frustration in the honeycomb lattice causes a phase transition from a long-range ordered locked phase over a floating phase with quasi long-range order and indications of a Berezinskii-Thouless-Kosterlitz-like character, to the thermally excited paramagnetic state. Absent spatial correlation and quasi pe-

riodic switching of isolated vortices in the quasi long-range ordered phase suggest a degeneracy of the vortex circulation.

Keywords

Macro spins; XY dipolar systems; phase transition; spin correlation; nano disk array; x-ray photoemission electron microscopy

Phase transitions, correlations and fluctuations of topological phases and vector spin frustrated systems have remained a fundamentally intriguing research problem for several decades.[1,2] In fact, advances in synthesizing systems with tailored chemical, electronic and/or magnetic disorder, and in characterization tools, including next generation diffraction limited light sources enabling *e.g.* element and magnetization sensitive x-ray photon correlation spectroscopy, combined with novel concepts of neural networks, quantum computing, and magnetic storage and logic devices, are expected to boost even further the interest in this research area. The appeal of geometric frustration is fueled by exotic physical behaviors originating from a macroscopic ground state degeneracy manifesting spin ices,[3–6] spin glasses,[7,8] quantum spin liquids,[9,10] vortices,[11–13] Skyrmions,[14–17] and Hopfions,[18,19] without the need of vector spin exchange, known as Dzyaloshinskii-Moriya interaction (DMI).[20,21] The continuous degeneracy of ideally frustrated systems is typically reduced by thermal fluctuations (spin wave excitation) and small imperfections to a discrete symmetry resembling the underlying structure. This phenomenon is referred to as "order-by-disorder"[13,22,23] and governs (quasi) long-range order in exchange and dipolar spin systems.[24] Though different in nature, theoretical and experimental data suggest that exchange and dipolar interaction may cause similarly frustrated states and phase transitions. While XY dipolar systems with square symmetry reveal a direct transition from an antiferromagnetic locked phase to a paramagnetic phase, honeycomb lattices are expected to exhibit an intermediate floating phase with quasi long-range order, vortex formation, and a Berezinskii-Thouless-Kosterlitz-like (BTK-

like) phase transition,[25] known from isotropic XY exchange systems.[11,12] The floating phase manifests due to spin frustration in the sense that not all spins can be collinear in the honeycomb ground states.[13,23] Structural disorder in imperfect square lattice may similarly lead to spin frustration and the nucleation of vortices.[26]

The original motivation to study spin frustrated XY dipolar systems traces back to $FeCl_3$-graphite intercalated compounds with strong dipolar and weak exchange interaction between layered Fe^{3+} ions arranged in a honeycomb lattice.[13] Despite successful correlation between experimental and numerical integral properties, a direct visualization of the predicted magnetization configurations in XY dipolar systems, providing an unambiguous proof, is still lacking three decades later.[13,23] More recently, the analogy between exchange and dipolar interactions in view of spin frustration was exploited to study artificial spin ice[6,27,28] and colloidal spin glass[29] at the micro scale through direct visualization of the magnetization configuration by fabricating arrays of magnetic planar micro-/nanostructures and magnetic colloids, respectively. Hybrid Ising-XY macro spin lattices resolved the inherent lack of degenerate ground states in planar artificial spin ice owing to distinct (next) nearest neighbor interactions.[30] To date, studies of XY macro spins had been limited to square lattices and the influence of (a relatively large) lattice spacing on their magnetization reversal processes[31,32] and thermal stability[33] retrieved from integral magnetometry measurements. The experimental challenge of preparing and investigating high-quality XY macro spin systems had yet to be overcome to visualize ground states and thermal fluctuations in square and particularly honeycomb lattices, which hold the promise of exciting physics. Recently, first steps have been undertaken to study thermal fluctuations and phase transitions in square lattices harnessing muon spin relaxation.[34]

Here, we investigate magnetic phases and correlations of planar XY macro spin lattices and report the experimental observation of magnetic ground states through direct imaging, predicted three decades ago.[13,23] As a model system, we use closely packed nano disk arrays with uniform magnetization, square and honeycomb symmetry, and various lattice constant.

The magnetization configurations are spatially resolved using x-ray photoemission electron microscopy (XPEEM, beamline 11.0.1 at the Advanced Light Source) in combination with x-ray magnetic circular dichroism (XMCD)[35,36] as element specific contrast mechanism. We observe the antiferromagnetic striped ground state in square lattices, and six-fold symmetric structures, *e.g.* trigonal vortex phase, disordered floating vortices, and indications of the thermally select paired ground state, in the honeycomb lattice. The spin configurations in the honeycomb lattice confirm the highly sensitive interplay between stray field interaction and thermal excitations (manipulated through enlarging lattice spacing and temperature) due to aforementioned spin frustration, that causes a phase transition from a long-range ordered locked phase over a floating phase with quasi long-range order to the thermally excited paramagnetic state. Vortices preferentially nucleate near domain boundaries or out of non-collinear spin configurations, *i.e.* vortices and disordered spins. We further show quasi periodic switching of the vortex circulation indicative of a degeneracy with respect to the sense of rotation. The stabilization of remanent striped domains in honeycomb lattices underlines the multipolar nature of the stray field interaction in closely packed nano disk arrays with an emergent magnetic hysteresis, which is absent in point-like XY dipolar systems.

The XY macro spin lattices were fabricated by lithographically patterning planar nano disk arrays and subsequent electron beam vapor deposition of soft-magnetic Permalloy (Py, $Ni_{80}Fe_{20}$) sandwiched between 2 nm titanium on naturally oxidized silicon wafers. Employing ultrasonic agitation development at 5°C to promote the removal of degraded molecules allowed for manufacturing holes with a spatial separation down to 30 nm and a shape as close to a circular disk as possible [Fig. 1]. The resulting iron-rich polycrystalline Permalloy ($Ni_{76}Fe_{24}$)[37] nano disks with a diameter of (100 ± 5) nm stabilize uniformly magnetized domains with minimal roughness related pinning, from here on referred to as XY macro spins. In particular, we prepared nano disk arrays with $\approx 10,000$ disks, lattice constant $a = (130 \sim 160)$ nm, thickness $h = (10 \pm 0.2)$ nm and diameter $d \simeq 100$ nm. Here, we focus on two specimens with $a = 150$ nm and $a = 155$ nm, which become thermally active

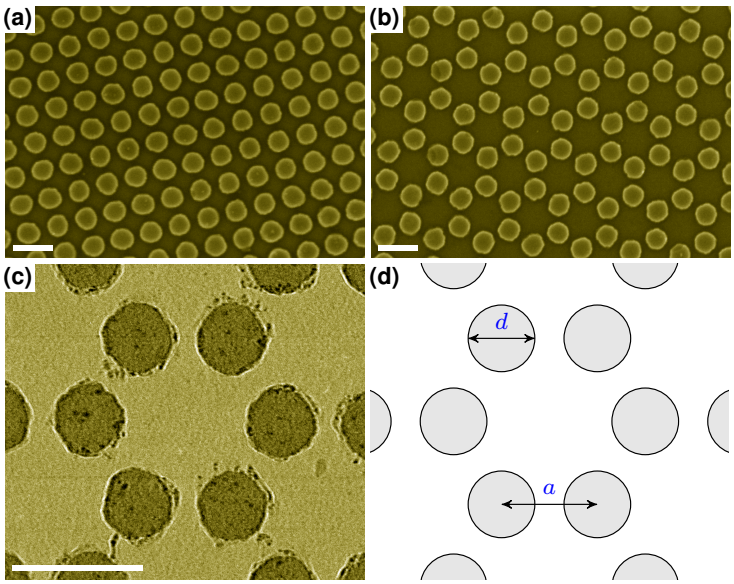

Figure 1: Nano disk arrays resembling XY macro spins. (a),(b) SEM (inlens) micrographs of square and honeycomb lattice. (c) TEM image revealing high-quality nano disks with traces of polymeric residuals. (d) Schematics of (c) indicating used notation. Scale bars are 200 nm.

slightly above room temperature. Numerous further investigations revealed a high sensitivity of the honeycomb lattice macro spins to spacing and structural imperfection that led to either highly fluctuating or locked spins in the entire accessible temperature range $(120 \sim 390)$ K given a temporal resolution of ≥ 2.5 s. The samples were mounted on a temperature controlled PEEM holder and *via* electromagnet *ex-situ* saturated perpendicularly to the magnetization sensitivity of XMCD and the short edge of the honeycomb lattice. This way, we avoided the influence of unknown conditions during growth on the as-grown magnetization configuration. We chose this orientation for two reasons regarding the honeycomb lattice: firstly, it provides the largest and most unambiguous contrast for the vortex configuration; and secondly, it minimizes the influence of field selection of frustrated spin configurations. The field was slowly ramped down, and the sample was taken out of the magnet such that the residual remanent field of the magnet acted in normal sample direction, minimizing its effect. Regarding the high-temperature measurements, the temperature was ramped up within 15 min and stabilized for at least 30 min. Afterwards, the PEEM was

realigned for 15 to 30 min to provide best possible contrast sensitivity and spatial resolution. The data were recorded over a period of about 30 min. The negligible energy barrier in the XY macro spins leads to an immediate response in form of the transition from *e.g.* remanent to thermally equilibrated states, which makes a precise time tracking unnecessary. This is in very contrast to artificial spin ice with a substantial energy barrier.

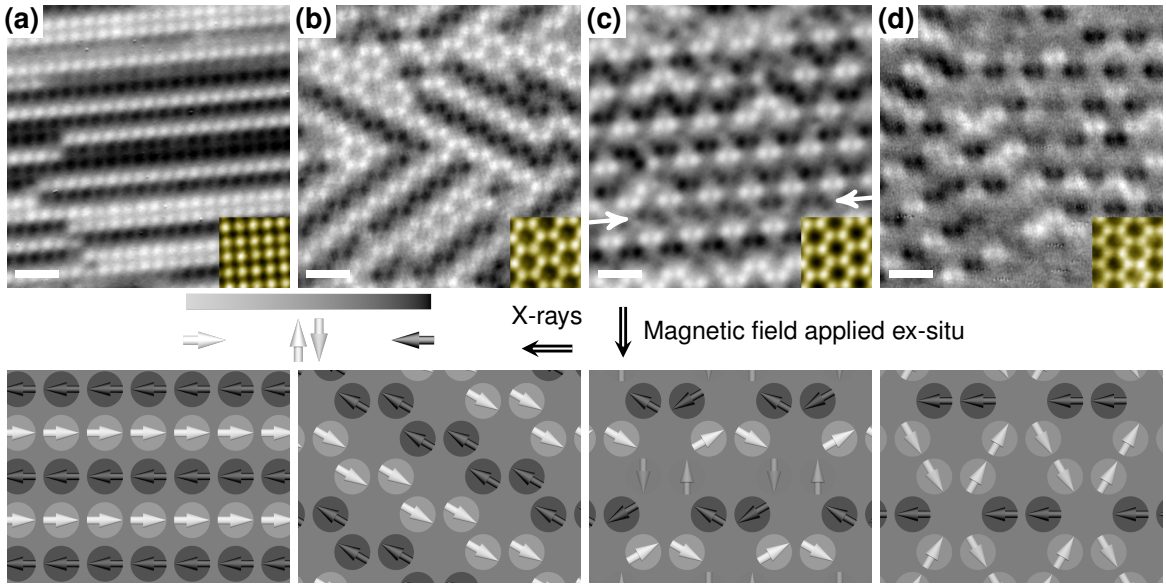

Figure 2: Ordering of magnetic XY macro spins in planar nano disk arrays ($h = 10\,\text{nm}$; $d = 100\,\text{nm}$; $a = 150\,\text{nm}$) visualized with XMCD-XPEEM. Each disk behaves as an (isotropic) XY macro spin which is magnetostatically coupled to its neighbors, resembling systems with (see schematics): (a),(b) uniaxial (striped) and (c),(d) six-fold symmetry, including two predicted honeycomb ground states: (c) vortices and (d) paired ground state. The white arrows in (c) indicate a region possibly in the paired ground state. The images display the remanent states at room temperature after *ex-situ* saturation along the indicated field direction, *e.g.* perpendicular to the short edge of the honeycomb lattice. Magnetic states shown in (b) and (c) are retrieved from different regions of the same nano disk array. Scale bars are 500 nm.

The room temperature remanent magnetization configuration of the macro spin ensembles may resemble domains with *e.g.* uniaxial and six-fold symmetry, including the vortex phase and paired ground state [Fig. 2], depending on saturation orientation relative to the lattice, temperature and structural properties, such as lattice symmetry, lattice constant and thickness. In the present case ($a = 150\,\text{nm}$, $h = 10\,\text{nm}$), the magnetostatic stray field

interaction, mediated through surface charges separated by $a - d \approx 50\,\mathrm{nm}$, is sufficiently strong to suppress thermal fluctuation at room temperature while preventing a completely saturated remanent state. Square lattices favor macro spin chains periodically alternating along the saturation direction with uniaxial (0°) [Fig. 2(a)] or biaxial (45°) symmetry. For either configuration, the corresponding thermally equilibrated state is a uniaxial system with long straight alternating stripes corresponding to the thermally select ground state of a XY dipolar square lattice,[23,24] that was recently also observed by muon spin relaxation.[34] It is worth to note that despite reordering of XY macro spins no persistent thermal fluctuations are observed in the square lattice at an elevated temperature of 390 K. The enhanced stability and correlation of square lattices with respect to the honeycomb lattice is an intrinsic property of the four-fold structural symmetry with a significant anisotropy,[23,24] which is further strengthened in closely packed lattices due to multipolar stray field interaction.[31] The associated hysteretic behavior originates from emergent energy barriers that may preserve magnetization configurations stabilized by an external in-plane magnetic field at remanence. For honeycomb lattices, this translates to a "ferromagnetic" state similar to striped domains, which, in ideal point-like XY dipolar systems with absent magnetic hysteresis, transforms at remanence into a six-fold symmetric vortex state.[13] The affinity towards either of the two ordered, symmetrically distinct states, namely striped [Fig. 2(b)] and theoretically predicted trigonal vortex phase [Fig. 2(c)], as remanent states depends on the interplay between thermal energy (temperature) and energy barrier (stray field interaction/spacing). For instance, room temperature honeycomb lattices consisting of Permalloy nano disks ($h = 10\,\mathrm{nm}$, $d = 100\,\mathrm{nm}$) with a spacing of $a - d \lesssim 50\,\mathrm{nm}$ and $a - d \gtrsim 50\,\mathrm{nm}$ prefer large striped domains (including single-domain states) and vortices (short-range ordered and disordered) as remanent states, respectively. A lattice constant of approximately 150 nm appears to balance the energy barrier between striped domain and vortex configuration, leading to a coexistence of both phases and the nucleation of extended trigonal vortex lattices at remanence [Figs. 2(b),(c); also Figs. 3(a),(b)]. Both displayed examples were retrieved from

different regions in the same honeycomb nano disk array during the same run, and qualitatively reproduced by others. Typically, the remanent striped domains expand over multiple nano disks and have a larger periodicity than those shown Figure 2(b). The increased vortex population and shrinking of striped domains at elevated temperatures discussed below confirms that individual energies are mostly unaffected. Each vortex lattice consists of the same number of vortices and antivortices forming pairs or ordered domains [schematics in Fig. 2(c)]. The term (anti-)vortex refers to the arrangement of adjacent XY macro spins, which is fundamentally different from soft-magnetic vortices observed in micro patterned films.[38] The absence of an out-of-plane magnetization component, usually referred to as (anti-)vortex core, in our systems is identical with the original BTK theory for 2D XY spin systems, lacking a third dimension. Moreover, we find indications of the thermally select ground state in honeycomb lattices [Fig. 2(d)], which we refer to as paired ground state due to collinearity of two neighboring XY macro spins.[23] This configuration is similar to the vortex phase characterized by a trigonal symmetry but causes an even weaker XMCD contrast [schematics in Fig. 2(d)]. Consequently, a definite proof can only be given by visualizing the complete in-plane magnetization component harnessing *e.g.* Lorentz microscopy[39] with exit wave reconstruction[40] or electron holography,[41] and is scope of future work. A closer look at the boundary between trigonal vortex lattices with opposite vortex circulation and lateral displacement of one hexagonal unit cell [region indicated by white arrows in Fig. 2(c); similar to upper right region in Fig. 3(a)] reveals a magnetization configuration similar to a vortex with tendency towards the paired ground state, which is the energetically preferable state due to minimized stray field contributions.

Despite great efforts to optimize the sample quality, our systems are far from being ideal. Both square and honeycomb lattices are ordered within few nanometers with nano islands exhibiting small deviations from perfect circular disks [Fig. 1]. These imperfections are in literature referred to as "dilution", and cause a random axis anisotropy[23] and local domains with same magnetization configurations. The impact is particularly strong in geometrically

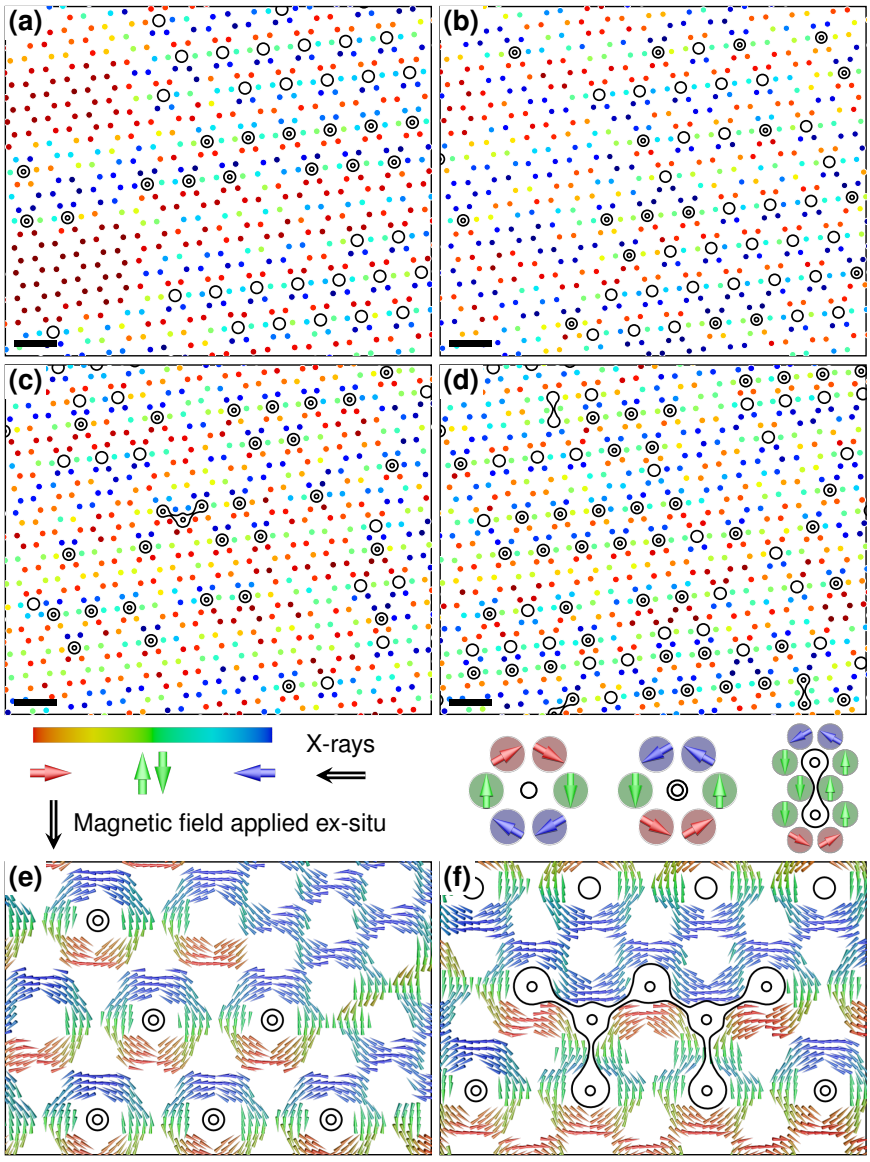

Figure 3: Remanent and thermally (partially) equilibrated states in honeycomb nano disk arrays measured at 300 K and 390 K, respectively. Panels (a)–(d) depict the time averaged in-plane magnetization component of each XY macro spin extracted from experimental data [(a),(b): $a = 150$ nm; (c),(d): $a = 155$ nm]. Thermal excitation at 390 K transforms the room temperature remanent states (a) and (c) into equilibrated states (b) and (d), respectively. The black circles indicate vortices formed by six XY macro spins (see schematics). Scale bars are 500 nm. (e),(f) Micromagnetic simulations reproducing coexistence of meander and vortex phase at remanence, *e.g.* trigonal lattice and higher order flux closure configurations.

frustrated honeycomb lattices, which additionally experience a preference of vortex state over paired ground state [Fig. 3].[23] While the majority of studied honeycomb lattices reveals either large striped domains, or individual vortices surrounded by striped domains or embedded in a bath of uncorrelated spins due to structural imperfection, select high-quality samples with tailored interaction ($a = 150\,\mathrm{nm}$) stabilize extended vortex lattices coexisting with striped domains at room temperature and remanence [Fig. 3(a)]. The ratio between phase coverage of striped domains and vortices is two to three in spite of local vortex lattice dominance. The slight increase in the lattice constant/spacing by 5 nm suppresses striped domains and increases vortex disorder [Fig. 3(c)]. Comparing these room temperature remanent states [Figs. 3(a),(c)] with their at 390 K thermally (partially) equilibrated states [Figs. 3(b),(d)] reveals three fundamental aspects: i) The initial net magnetic moment of the remanent states due to a slight misalignment of 5° vanishes upon thermal equilibration, leaving an XMCD distribution characteristic for vortex formation [Fig. 4(a)]; ii) The lateral size of striped domains if existent is significantly reduced from $> 10\,a$ to $\approx 1\,a$ [left side of Figs. 3(a),(b)]; iii) The vortex phase is preserved, but laterally rearranged, underlining the absence of (significant) structural pinning, and its "floating" characteristics during thermalization, that draws similarities to spin liquids and BTK-like transitions. We refer to the alternation of the magnetization in this specific manner (more details below) as partial equilibration due to the lack of a global phase homogeneity as expected for a complete thermal equilibration. However, all thermally (partially) equilibrated states exhibit an increased vortex population with respect to their room temperature remanent states. This is particularly evident in disordered vortex phases ($a = 155\,\mathrm{nm}$), where the vortex phase coverage soars from 39% to 59% [Figs. 3(c),(d)]. With increasing vortex population/density, the initial randomness turns into short-range order with different local symmetries, *i.e.* trigonal and square lattices [Figs. 3(c),(d); Fig. 4(b)]. In contrast, an originally ordered vortex lattice with slightly stronger interaction ($a = 150\,\mathrm{nm}$) may coherently expand [Figs. 3(a),(b); Fig. 4(b)]. Comparing the first two peaks of the radial vortex distribution normalized to the vortex

phase coverage provides means to quantify the growth of the trigonal and square configuration [Fig. 4(b)]. In particular, the ratio between short-range order with trigonal and square symmetry decreases from 11.5 to 5.8 for the disordered vortex phase [Figs. 3(c),(d)], which is equal to a growth of 50% and 200% for trigonal and square lattice, respectively. Note that the apparent preference of square configuration is due to its initial negligibility. The absolute growth and coverage of the trigonal vortex lattice is for any investigated sample larger compared to the square lattice [Fig. 4(b)]. Indeed, the thermally equilibrated state of the originally ordered vortex lattice [Figs. 3(a),(b)] shows no square symmetry at all, but a significant increase (2×) of higher order peaks, indicating long-range order.

The preference of trigonal over square vortex lattices in XY dipolar systems with honeycomb symmetry can be explained based on magnetic flux closure, which is best for closely packed trigonal arrangements due to constant orientation of the XY macro spin with respect to the center of each vortex [schematics in Fig. 2(c)]. This feature draws similarities to Skyrmion lattices occurring in B20 inversion symmetry broken single crystals[42] with DMI. The qualitative explanation is confirmed by rigorous theoretical description of XY dipolar systems[13,23] and for finite nano disks by micromagnetic simulations calculating the energy and relaxed states of vortex lattices with various symmetries ($h = 10\,\mathrm{nm}$; $d = 100\,\mathrm{nm}$; $a = 150\,\mathrm{nm}$; $M_s = 860\,\mathrm{kA/m}$; $A = 13\,\mathrm{pJ/m}$). Briefly, the stray field energy for square lattices is twice the value of trigonal vortex lattices and striped domains. Contributions directly associated with the finite size of the nano disks, such as small distortions of the magnetization (non-uniformity) near the edges [Figs. 3(e),(f)], play a minor role since they do not discriminate between striped domains and trigonal vortex lattices. Furthermore, micromagnetic simulations reproduced the experimentally observed remanent states with coexisting nearly degenerate striped and vortex phase (and higher order flux closure domains) at remanence [Figs. 3(e),(f)]. The simulations performed at 0 K reveal a selection of one circulation in the vortex lattice, which originates from stray field minimization during the nucleation process, and agrees well with theoretical predictions of homocircular vortex lattices.[13,23] Such a pref-

erence is experimentally confirmed by observing spatially confined vortex lattices with same sense of circulation at remanence, split up into domains due to numerous nucleation sites [Fig. 3(a)]. Contrary to the field-driven transitions (remanent state) [Figs. 3(a),(c)], thermal equilibration does not discriminate between vortex circulations [Figs. 3(b),(d)], as evident from an integral change of $\lesssim 5\%$, and a vanishing vortex circulation correlation function $C_1(r \gtrsim 3.5a) = \langle c(\vec{R})c(\vec{R}+\vec{r})\rangle_{\vec{R}} \approx 0.01$ (excluding nearest neighbors) for the disordered vortex phase [Fig. 3(d)]. The vortex circulation $c(\vec{R})$ is defined as ± 1 for opposite circulation, and 0 for absent vortices. Furthermore, $\vec{R} = (x, y)$ and $\vec{r}$ is the location of vortices, *i.e.* center of hexagon, and the distance vector, respectively.

On the other hand, calculating the vortex correlation function $C_2(r) = 3\langle c^2(\vec{R})c^2(\vec{R}+\vec{r})\rangle_{\vec{R}}$ allows for quantifying the aforementioned (quasi) long-range order as the vortex population increases, and identifying the nature of the phase transition. The coefficient normalizes $C_2(r)$ to the vortex population $C_2(0)$ of a perfect trigonal lattice. Please note that we calculate the radial vortex correlation instead of the commonly used spin-spin correlation after gauge transformation into a uniformly magnetization state[24] due to the lack of knowledge about the second in-plane magnetization component. This approximation is valid since the phase transitions are characterized by vortex formation. Because the phase transition is approached from below the critical temperature, the correlation function is expected to follow either an exponential or algebraic spatial dependence for conventional ordering transition and BTK transition,[11,12] respectively. The resulting long-range order ($C_2(r) \propto e^{-\frac{r}{\xi}}$) and quasi long-range order ($C_2(r) \propto r^{-\eta}$), respectively, can be discriminated by plotting the vortex correlation function on loglog [Fig. 4(c)] and semilogy [Fig. 4(d)] scale. Analyzing the vortex correlation length ξ of the ordered vortex phase reveals $\xi = (5.5 \pm 0.2)\, a$ for the room temperature remanent state, and $\xi = (10.9 \pm 0.6)\, a$ for the at 390 K thermally equilibrated state [Figs. 3(a),(b)]. The relative growth is similar to the increase of higher order peaks in the radial vortex distribution associated with trigonal symmetry [Fig. 4(b)]. Contrarily, the disordered vortex phase exhibits a rapid drop of the vortex correlation function for small

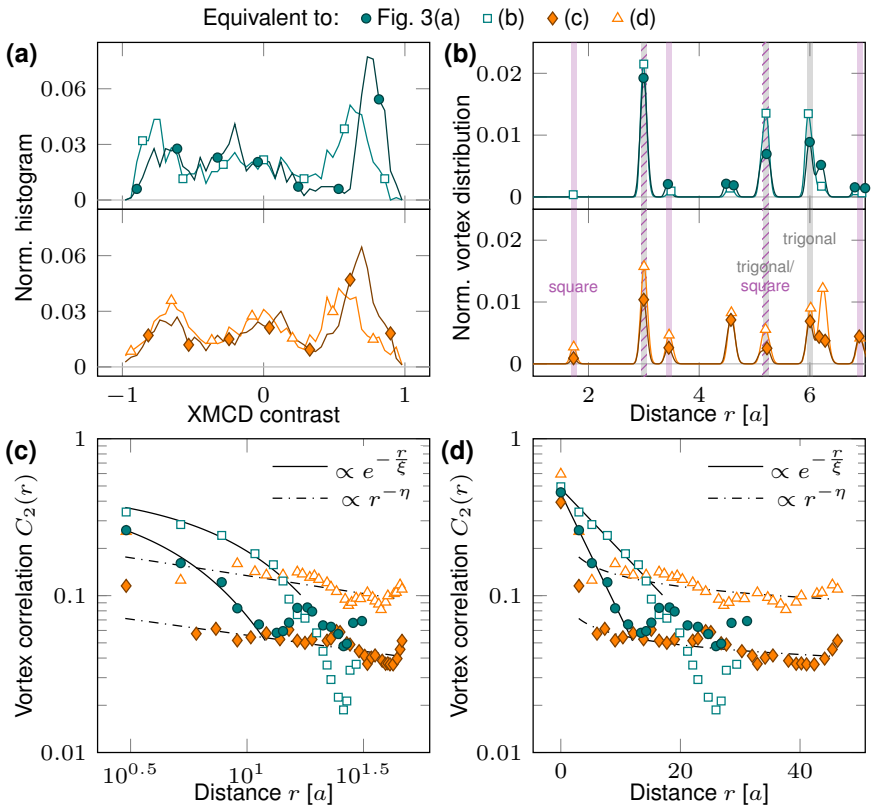

Figure 4: Spatial correlation of vortex phase in honeycomb lattices. (a) XMCD contrast distribution revealing initial bias of remanent states due to 5° misalignment, and balancing of thermally equilibrated states, characteristic for vortex formation. (b) Radial vortex distribution normalized to the vortex phase coverage $C_2(0)$ quantifies growth of trigonal vortex lattice and mutual increase of trigonal and square configuration in the disordered phase. Vertical lines indicate peak positions associated with square and trigonal symmetry, or both. (c),(d) Radial vortex correlation function $C_2(r)$ plotted on loglog and semilogy scale reveals an increased long-range and quasi long-range order for thermally equilibrated states with prior ordered and disordered vortex phase, respectively. $C_2(0)$ refers to the vortex population/vortex phase coverage. Vortex distribution and correlation function are given in units of the lattice constant a.

distances due to short-range order, followed by an algebraic decay with $\eta = 0.2 \pm 0.1$ and $\eta = 0.23 \pm 0.1$ for room temperature remanent and thermally equilibrated states, respectively [Figs. 3(c),(d)]. Although these η values are close to the theoretical value of 0.25 at the BTK transition,[11,12] experimental uncertainty primarily limited by statistics does not provide definite proof. However, the failure of an exponential fit and the enlarged overall correlation of the thermally (partially) equilibrated state are indicators of a BTK-like transition occurring in the XY honeycomb lattices at slightly higher temperatures.

While the presented samples ($a \lesssim 155\,\mathrm{nm}$) are thermally stable at room temperature and do not reveal any noticeable change for multiple hours, an elevated temperature of 390 K thermally (partially) equilibrates the states, reducing net magnetic moment, enlarging vortex population, and inducing a quasi long-range order in the disordered floating phase [Fig. 4]. In order to probe the governing role of stray field interaction and associated time scales, we monitor thermal fluctuations by analyzing subsequent image series. The photon helicity is changed every ten images, enabling us to retrieve both time averaged XMCD signal ($\sim 30\,\mathrm{min}$) and temporal evolution to discriminate between spatially varying projection angle and thermal fluctuations with a temporal resolution of $(7 + 0.5)\,\mathrm{s}$, including readout time. While this exposure time is sufficient for probing ensembles with $a \lesssim 155\,\mathrm{nm}$ at 390 K, spin fluctuations in lattices with $a \gtrsim 160\,\mathrm{nm}$ exceed the temporal resolution limit of 2.5 s, leading to apparently uncorrelated system. We did not apply aberration correction, demonstrated to enhance spatial resolution and contrast levels,[43] due to yet unknown long-term stability. In particular, the transition may occur abruptly ($< 4\,\mathrm{s}$, equal to half the acquisition time) or slowly, similar to domain wall creeping, over tens of minutes. The latter is a prominent mechanism for the homogeneous domains splitting up into striped domains that advance from the border inwards without breaking flux closure (symmetry). Nucleations of symmetrically distinct states, *i.e.* vortices and higher order flux closure domains that ultimately transform into striped domains, have been observed within homogeneous domains, though less frequently. In fact, these states preferentially stabilize near domain boundaries

and out of non-collinear spin configurations, *e.g.* vortex and disordered phases [Fig. 3]. Aside from uncorrelated infrequent fluctuations, we observe subsequent vortex circulation switching in the quasi long-range ordered phase in the vicinity of an otherwise thermally stable XY lattice ($a = 155\,\mathrm{nm}$) [Figs. 5(a),(b)]. To quantify the switching, we calculate the temporal auto correlation function $G(t) = \sum_j^N \langle S_x(\vec{R}_j, \tau) S_x(\vec{R}_j, \tau + t) \rangle_\tau$, where S_x is the magnetization component along the x-ray trajectory (XMCD contrast) of individual nano disks located at $\vec{R}_j$. It is calculated as the sum over the two top nano disks minus the sum over the two bottom nano disks, that serves as a measure for the magnetic vortex state. The two center nano disks exhibit a virtually vanishing contrast due to perpendicular macro spin alignment with respect to the x-ray trajectory. The corresponding correlation $G(t)$ quantitatively confirms the quasi periodic switching of the vortex circulation [Fig. 5(c)] in the floating vortex phase [Fig. 3(d)], and the corresponding degeneracy of vortex circulation.

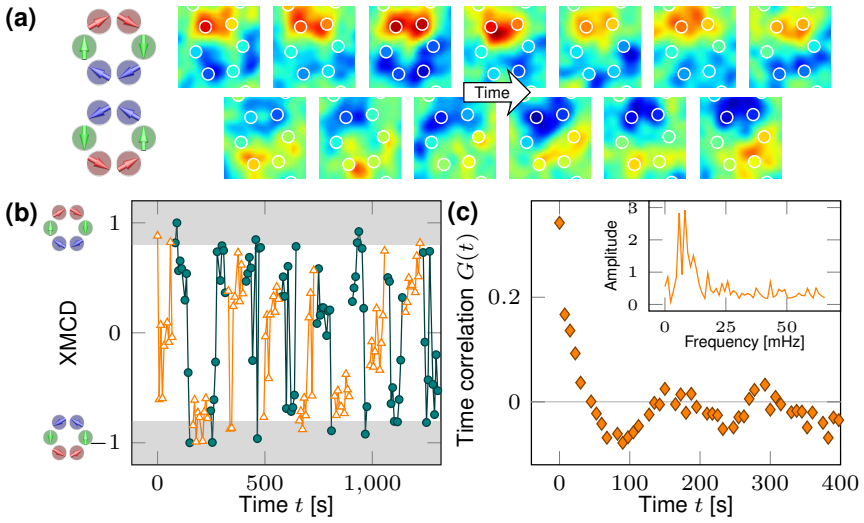

Figure 5: Temporal evolution of vortex switching in quasi long-range ordered vortex phase at 390 K. (a) Image series illustrating subsequent, collective vortex circulation switching. Background shows the raw XMCD data overlaid by white circles referring to the XMCD data of individual XY macro spins. (b) In-plane magnetization component as a function of time with temporal resolution of 7.5 s. Orange and green curves refer to opposite photon helicity. (c) Auto correlation function revealing quasi periodic switching. Maximal correlation is equal to 0.66.

In conclusion, we studied spin configurations, correlations and fluctuations in planar

XY macro spin lattices resembling XY dipolar systems at the micro scale. We observed the theoretically predicted antiferromagnetic striped ground state in square lattices, and six-fold symmetric structures, such as trigonal vortex lattices, disordered floating vortices, and indications of the thermally select paired ground state, in the honeycomb lattice. The emergence of striped domains originates from the hysteretic behavior of XY macro spin systems owing to multipolar stray field interaction that preserves in-field stabilized states at remanence. The increased vortex population and shrinking/collapse of striped domains at elevated temperatures confirms that individual energies are mostly unaffected. The spin frustration in honeycomb lattices causes a phase transition from a long-range ordered locked phase over a floating phase with quasi long-range order of vortices, similarly to the BTK transition, to the paramagnetic state. The governing interplay between stray field interaction and thermal excitations was manipulated through enlarging lattice spacing and temperature. Furthermore, quasi periodic switching of isolated vortices and absent correlation except for nearest neighbors (short-range order) in the quasi long-range ordered phase confirmed the degeneracy of the vortex circulation. Our results prove the possibility to fabricate and investigate XY dipolar systems at the micro scale, and open up a new avenue in the field of artificial spin ice towards XY spins, spin liquids, Kitaev's XYZ honeycomb lattices, and magnonics with tunable interactions.

Acknowledgement

This work was primarily funded by the U.S. Department of Energy, Office of Science, Basic Energy Sciences, Materials Sciences and Engineering Division under Contract No. DE-AC02-05-CH11231 within the NEMM program (MSMAG). Work at the Molecular Foundry was supported by the U.S. Department of Energy, Office of Science, Basic Energy Sciences

under Contract No. DE-AC02-05-CH11231. This research used resources of the Advanced Light Source, which is a DOE Office of Science User Facility under contract no. DE-AC02-05CH11231.

References

(1) De'Bell, K.; MacIsaac, A. B.; Whitehead, J. P. Dipolar effects in magnetic thin films and quasi-two-dimensional systems. *Rev. Mod. Phys.* **2000**, *72*, 225–257.

(2) Batista, C. D.; Lin, S.-Z.; Hayami, S.; Kamiya, Y. Frustration and chiral orderings in correlated electron systems. *Rep. Prog. Phys.* **2016**, *79*, 084504.

(3) Harris, M. J.; Bramwell, S. T.; McMorrow, D. F.; Zeiske, T.; Godfrey, K. W. Geometrical Frustration in the Ferromagnetic Pyrochlore $Ho_2Ti_2O_7$. *Phys. Rev. Lett.* **1997**, *79*, 2554–2557.

(4) Ramirez, A. P.; Hayashi, A.; Cava, R. J.; Siddharthan, R.; Shastry, B. S. Zero-point entropy in 'spin ice'. *Nature* **1999**, *399*, 333.

(5) Bramwell, S.; Gingras, J. Spin Ice State in Frustrated Magnetic Pyrochlore Materials. *Science* **2001**, *294*, 1495.

(6) Wang, R. F.; Nisoli, C.; Freitas, R. S.; Li, J.; McConville, W.; Cooley, B. J.; Lund, M. S.; Samarth, N.; Leighton, C.; Crespi, V. H.; Schiffer, P. Artificial "spin ice" in a geometrically frustrated lattice of nanoscale ferromagnetic islands. *Nature* **2006**, *439*, 303.

(7) Sherrington, D.; Kirkpatrick, S. Solvable Model of a Spin-Glass. *Phys. Rev. Lett.* **1975**, *35*, 1792–1796.

(8) Binder, K.; Young, A. P. Spin glasses: Experimental facts, theoretical concepts, and open questions. *Rev. Mod. Phys.* **1986**, *58*, 801–976.

(9) Anderson, P. Resonating valence bonds: A new kind of insulator? *Mater. Res. Bull.* **1973**, *8*, 153 – 160.

(10) Zhou, Y.; Kanoda, K.; Ng, T.-K. Quantum spin liquid states. *Rev. Mod. Phys.* **2017**, *89*, 025003.

(11) Berenzinskii, V. Destruction of long-range order in one-dimensional and two-dimensional systems possessing a continuous symmetry group. II. Quantum systems. *Sov. Phys. JETP* **1972**, *34*, 610–616.

(12) Kosterlitz, J. M.; Thouless, D. J. Ordering, metastability and phase transitions in two-dimensional systems. *J. Phys. C: Solid State Phys.* **1973**, *6*, 1181.

(13) Zimmerman, G. O.; Ibrahim, A. K.; Wu, F. Y. Planar classical dipolar system on a honeycomb lattice. *Phys. Rev. B* **1988**, *37*, 2059–2065.

(14) Roessler, U. K.; Bogdanov, A. N.; Pfleiderer, C. Spontaneous skyrmion ground states in magnetic metals. *Nature* **2006**, *442*, 797.

(15) Okubo, T.; Chung, S.; Kawamura, H. Multiple-q States and the Skyrmion Lattice of the Triangular-Lattice Heisenberg Antiferromagnet under Magnetic Fields. *Phys. Rev. Lett.* **2012**, *108*, 017206.

(16) Leonov, A. O.; Mostovoy, M. Multiply periodic states and isolated skyrmions in an anisotropic frustrated magnet. *Nat. Commun.* **2015**, *6*, 8275.

(17) Zhang, X.; Xia, J.; Zhou, Y.; Liu, X.; Zhang, H.; Ezawa, M. Skyrmion dynamics in a frustrated ferromagnetic film and current-induced helicity locking-unlocking transition. *Nat. Commun.* **2017**, *8*, 1717.

(18) Ackerman, P. J.; Smalyukh, I. I. Static three-dimensional topological solitons in fluid chiral ferromagnets and colloids. *Nat. Mater.* **2016**, *16*, 426.

(19) Sutcliffe, P. Skyrmion Knots in Frustrated Magnets. *Phys. Rev. Lett.* **2017**, *118*, 247203.

(20) Dzyaloshinskii, I. E. Thermodynamic theory of weak ferromagnetism in antiferromagnetic substances. *Sov. Phys. JETP* **1957**, *5*, 1259.

(21) Moriya, T. Anisotropic Superexchange Interaction and Weak Ferromagnetism. *Phys. Rev.* **1960**, *120*, 91–98.

(22) Villain, J.; Bidaux, J. P., R. Carton; Conte, R. Ordering due to disorder in dipolar magnets on two-dimensional lattices. *J. Phys. (Paris)* **1980**, *41*, 1263.

(23) Prakash, S.; Henley, C. L. Ordering due to disorder in dipolar magnets on two-dimensional lattices. *Phys. Rev. B* **1990**, *42*, 6574–6589.

(24) De'Bell, K.; MacIsaac, A. B.; Booth, I. N.; Whitehead, J. P. Dipolar-induced planar anisotropy in ultrathin magnetic films. *Phys. Rev. B* **1997**, *55*, 15108–15118.

(25) Baek, S. K.; Minnhagen, P.; Kim, B. J. Kosterlitz-Thouless transition of magnetic dipoles on the two-dimensional plane. *Phys. Rev. B* **2011**, *83*, 184409.

(26) Schildknecht, D.; Heyderman, L. J.; Derlet, P. M. Phase diagram of dipolar-coupled XY moments on disordered square lattices. *Phys. Rev. B* **2018**, *98*, 064420.

(27) Morgan, J. P.; Langridge, S.; Marrows, C. H. Thermal ground-state ordering and elementary excitations in artificial magnetic square ice. *Nat. Phys.* **2011**, *7*, 75.

(28) Mengotti, E.; Heyderman, L.; Rodriguez, A.; Nolting, F.; Hugli, R.; Braun, H.-B. Real-space observation of emergent magnetic monopoles and associated Dirac strings in artificial kagome spin ice. *Nat. Phys.* **2011**, *7*, 68.

(29) Zhou, D.; Wang, F.; Li, B.; Lou, X.; Han, Y. Glassy Spin Dynamics in Geometrically Frustrated Buckled Colloidal Crystals. *Phys. Rev. X* **2017**, *7*, 021030.

(30) Östman, E.; Stopfel, H.; Chioar, I.-A.; Arnalds, U. B.; Stein, A.; Kapaklis, V.; Hjörvarsson, B. Interaction modifiers in artificial spin ices. *Nat. Phys.* **2018**, *14*, 375–379.

(31) Vedmedenko, E. Y.; Mikuszeit, N.; Oepen, H. P.; Wiesendanger, R. Multipolar Ordering and Magnetization Reversal in Two-Dimensional Nanomagnet Arrays. *Phys. Rev. Lett.* **2005**, *95*, 207202.

(32) Ewerlin, M.; Demirbas, D.; Brüssing, F.; Petracic, O.; Ünal, A. A.; Valencia, S.; Kronast, F.; Zabel, H. Magnetic Dipole and Higher Pole Interaction on a Square Lattice. *Phys. Rev. Lett.* **2013**, *110*, 177209.

(33) Arnalds, U. B.; Ahlberg, M.; Brewer, M. S.; Kapaklis, V.; Papaioannou, E. T.; Karimipour, M.; Korelis, P.; Stein, A.; lafsson, S. O.; Hase, T. P. A.; Hjörvarsson, B. Thermal transitions in nano-patterned XY-magnets. *Appl. Phys. Lett.* **2014**, *105*, 042409.

(34) Leo, N.; Holenstein, S.; Schildknecht, D.; Sendetskyi, O.; Luetkens, H.; Derlet, P. M.; Scagnoli, V.; Lançon, D.; Mardegan, J. L.; Prokscha, T.; Suter, A.; Salman, Z.; Lee, S.; Heyderman, L. J. Collective magnetism in an artificial 2D XY spin system. *Nat. Commun.* **2018**, *9*, 2850.

(35) Chen, C. T.; Sette, F.; Ma, Y.; Modesti, S. Soft-x-ray magnetic circular dichroism at the $L_{2,3}$ edges of nickel. *Phys. Rev. B* **1990**, *42*, 7262–7265.

(36) Thole, B. T.; Carra, P.; Sette, F.; van der Laan, G. X-ray circular dichroism as a probe of orbital magnetization. *Phys. Rev. Lett.* **1992**, *68*, 1943–1946.

(37) Streubel, R.; Lee, J.; Makarov, D.; Im, M.-Y.; Karnaushenko, D.; Han, L.; Schäfer, R.; Fischer, P.; Kim, S.-K.; Schmidt, O. G. Magnetic Microstructure of Rolled-Up Single-Layer Ferromagnetic Nanomembranes. *Adv. Mater.* **2014**, *26*, 316–323.

(38) Velten, S.; Streubel, R.; Farhan, A.; Kent, N.; Im, M.-Y.; Scholl, A.; Dhuey, S.; Behncke, C.; Meier, G.; Fischer, P. Vortex circulation patterns in planar microdisk arrays. *Appl. Phys. Lett.* **2017**, *110*, 262406.

(39) Phatak, C.; Petford-Long, A. K.; Heinonen, O.; Tanase, M.; De Graef, M. Nanoscale structure of the magnetic induction at monopole defects in artificial spin-ice lattices. *Phys. Rev. B* **2011**, *83*, 174431.

(40) Streubel, R.; Lambert, C.; Kent, N.; Ercius, P.; N'Diaye, A. T.; Ophus, C.; Salahuddin, S.; Fischer, P. Experimental Evidence of Chiral Ferrimagnetism in Amorphous GdCo Films. *Adv. Mater. 30*, 1800199.

(41) Lichte, H.; Lehmann, M. Electron holography - basics and applications. *Rep. Prog. Phys.* **2008**, *71*, 016102.

(42) Yu, X. Z.; Onose, Y.; Kanazawa, N.; Park, J. H.; Han, J. H.; Matsui, Y.; Nagaosa, N.; Tokura, Y. Real-space observation of a two-dimensional skyrmion crystal. *Nature* **2010**, *465*, 901–904.

(43) Scholl, A.; Marcus, M.; Doran, A.; Nasiatka, J.; Young, A.; MacDowell, A.; Streubel, R.; Kent, N.; Feng, J.; Wan, W.; Padmore, H. Hartmann characterization of the PEEM-3 aberration-corrected X-ray photoemission electron microscope. *Ultramicroscopy* **2018**, *188*, 77.

Graphical TOC Entry